IEEE Access
Multidisciplinary | Rapid Review | Open Access Journal

Received April 9, 2019, accepted May 11, 2019, date of publication May 17, 2019, date of current version June 19, 2019.

Digital Object Identifier 10.1109/ACCESS.2019.2917529

Dual-Switch Boost DC–DC Converter for Use in Fuel-Cell-Powered Vehicles

XIAOGANG WU[1], WENWEN SHI[1], AND JIUYU DU[2]

[1]School of Electrical and Electronic Engineering, Harbin University of Science and Technology, Harbin 150080, China
[2]State Key Laboratory of Automotive Safety and Energy, Tsinghua University, Beijing 100084, China

Corresponding author: Jiuyu Du (dujiuyu@tsinghua.edu.cn)

This work was supported in part by the National Key Technologies R&D Program of MOST under Grant 2018YFB0105403, in part by the University Nursing Program for Young Scholars with Creative Talent in Heilongjiang Province under Grant UNPYSCT-2016164, and in part by the Fundamental Research Foundation for Universities of Heilongjiang Province under Grant LGYC2018JQ005.

ABSTRACT To facilitate voltage matching between the cell stack and power batteries in fuel-cell-powered vehicles, an implementation of a simple dual-switch boost DC–DC converter topology has been proposed in this paper. Compared with existing boost topologies, the one proposed herein reduces the number of components required and stress induced whilst maintaining a high-gain ratio. The results of experiments performed in this paper reveal that the corresponding to a duty ratio of 0.8, the proposed converter topology demonstrates the realization of a boost ratio of 6, thereby exceeding that the realized by conventional boost converters by nearly 73%. In addition, at an output voltage of 50 V, a maximum operating efficiency of 91% was achieved. These results demonstrate the effectiveness and feasibility of the proposed DC–DC converter topology for use in fuel-cell-powered vehicles.

INDEX TERMS Fuel cell, DC/DC converter, topology, high gain ratio.

I. INTRODUCTION

Voltage matching between the fuel cell and auxiliary power supply along with improvement in fuel-cell output-voltage characteristics constitutes the primary function of DC–DC converters employed in electric automotive applications [1], [2]. DC–DC converters are traditionally employed to regulate fuel-cell output power by controlling the switching operation (on and off) of the power switch. Efficient operation of fuel cells requires accurate matching of their output voltage with a DC bus. Additionally, suppression of ripples within the fuel-cell output current must also be ensured to prolong their operating life [3]. Unlike lithium ion batteries, fuel cell output voltage fluctuates greatly, output characteristics are weak, and output power fluctuates greatly, which makes it difficult to meet the needs of lift vehicles. Therefore, the DC/DC converter for fuel cell is different from that for lithium ion battery, which is mainly reflected in its stable operation in a wider range and faster response speed. It is difficult to design the topology of the DC/DC converter for fuel cell. In view of these requirements, DC–DC converters developed for use in fuel-cell applications must demonstrate high operating efficiency, high boost ratio, high power density, small input-current ripple, and stable operation over long operating periods [4], [5].

With regard to extant researches concerning the development of DC–DC converter topology for use in fuel-cell applications, a buck–boost DC–DC converter with continuous input current was proposed in [6]. Operation of the said converter could be controlled by means of a single switch, and the voltage-induced stress across the switch was observed to be very low. A zero-voltage switching (ZVS) three-phase current-feed push-pull converter was presented in [7] to facilitate realization of ZVS of all main switches and zero-current switching (ZCS) of secondary diodes, thereby enhancing the conversion efficiency. Compared to existing three-phase current-fed push-pull converters employing a voltage clamp, a much simpler active-clamp circuit was employed in [7] to repeatedly use the leakage inductance for soft commutation as well as suppression of the transient surge voltage. A low voltage could, therefore, be achieved using a switch with a low ''ON''-state resistance. A non-isolated ZVS interleaved DC–DC boost converter was proposed in [8]. In this design, the energy stored within the leakage inductor could be recycled using a coupled inductor and active-clamp circuit. In addition, the ZVS ''ON'' state of the main and clamp switches could be realized. As reported in [8], the active-clamp circuit suppressed voltage

The associate editor coordinating the review of this manuscript and approving it for publication was Rui Xiong.

spikes observed on main switches, whereas the voltage drop across the clamp capacitor resulted in higher voltage gain. In [9], an isolated, bidirectional, dual-active bridge, series-resonant DC–DC converter was proposed based on switching impedance. The said converter could facilitate full-range soft switching of all switches, thereby reducing switching losses. Power control was achieved via tuning of switching capacitors that constituted the series-resonant tank circuit. In [10], a nonisolated, high-boost DC–DC converter was proposed based on the current-fed Cockcroft–Walton voltage multiplier (CW-VM). The topology of the said converter comprised two low-voltage, common-emitter switches. The current-fed CW-VM was primarily used eliminate such problems associated with its conventional voltage-fed counterparts as inadequate suppression of voltage ripples and load-related voltage drops. An H-structure boost, three-level DC–DC converter (HS-BTL) with a wide voltage-gain range was proposed in [11], and its performance was compared against that of a conventional flying-capacitor boost, three-level DC–DC converter. The proposed converter demonstrated realization of a high voltage gain without the need for complex control of the flying-capacitor voltage balance. A new and improved LLC converter with two separate resonant branches for wide input-voltage-range applications was proposed [12]. The said converter could operate in the low-gain (LG) or medium-gain (MG) modes. The observed voltage gain during operation in the MG mode was observed to be 1.5 times that during operation in the LG mode. By operating the converter in different modes, the input voltage could be adjusted over a wide range. A single-switch boost DC–DC converter equipped with a diode-capacitor module was proposed in [13]. In this design, all capacitors were charged in parallel and discharged in series, and a wide voltage-gain range was realized through use of a simple structure. In [14] was proposed a wide-range ZVS active-clamp current-fed push-pull converter for use in fuel-cell applications. The said converter design was intended to realize ZVS and ZCS for all primary switches and secondary diodes, respectively, from rated load to 10% of the full load over a wide range of input-voltage variations, thereby increasing the overall conversion efficiency. Lastly, a parallel-input series-output DC–DC boost converter was proposed in [15]. The said converter could operate over a wide input-voltage range, and it possessed an interleaved structure on the input side to facilitate suppression of ripples within the input current. During series operation of the said converter, a high voltage gain was achieved.

In conclusion, most extant studies concerning DC–DC-converter topologies for use in fuel-cell-powered vehicles focused on improving either the conversion efficiency—via adoption of ZVS and ZCS—or converter gain—by changing the series–parallel form of the input and output circuits to facilitate suppression of current ripples [16]. As regards the practical application of fuel-cell-powered vehicles, the structure of and voltage stress induced within converters must be simplified to enhance their conversion reliability. In this study, a dual-switch boost DC–DC converter structure was adopted to facilitate accurate voltage matching between the fuel cell and power battery. The proposed converter topology demonstrates characteristics of low output-voltage ripple, low power-device stress, and high efficiency. The two switches of the two-switch boost converter are turned on or off at the same time, compared with the phase-shifting control of interleaved converter, the control of this converter is relatively simple. In addition, the dual-switch boost converter has the advantages of less devices, small circuit size, and low cost [17].

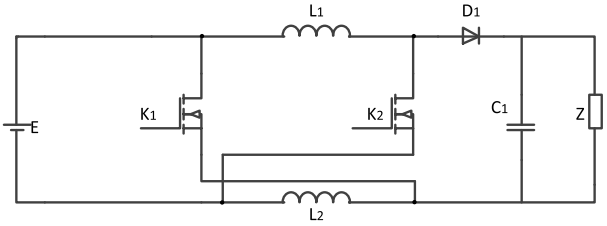

FIGURE 1. Proposed dual-switch boost DC–DC converter topology.

II. CONVERTER TOPOLOGY

A schematic of the proposed dual-switch boost DC–DC converter topology is depicted in Fig. 1. It comprises two MOSFET power switches (K_1 and K_2), two energy-storage inductors (L_1 and L_2), a diode D_1, and an output filter capacitor C_1. The two power-switch tubes were capable of being simultaneously turned on or off. As can be observed, the proposed topology possesses a simple structure, and the boost voltage was observed to be relatively high, thereby meeting the basic requirements of DC–DC converter topologies intended for use in fuel-cell-powered vehicles.

Assuming each circuit component in Figure 1 to be ideal, magnitudes of inductances L_1 and L_2 can be determined to be equal. Likewise, values of parameters concerning MOSFETs K_1 and K_2 can be determined to be equal, thereby facilitating them to switch ON and OFF simultaneously. This ON and OFF switching of the two MOSFETs corresponds to realization of different operating states of the converter circuit.

When switches K_1 and K_2 are set in the ON state, the working mode of the proposed converter can be described as depicted in Fig. 2(a). There exist two current loops within the circuit. The first loop comprises series arrangements of K_1–L_2 and K_2–L_1 connected in parallel across the input power supply E. The filter capacitor C_1 in combination with load Z constitutes the second loop. Ignoring the voltage drop across MOSFETs in the ON state, the equivalent converter circuit under the working mode can be reduced to the form depicted in Figure 2(b), wherein inductors L_1 and L_2 are considered equivalent to two current sources, the voltage corresponding to which is equivalent to the input supply voltage E. Additionally, directions of the said voltage and current were considered to align with reference directions depicted in the figure, corresponding to the time over which the inductor absorbs energy. In one cycle, the two switches remain in the ON state over a duration $D \times TS$, where D denotes the PWM duty cycle. If the inductor currents are assumed constant and

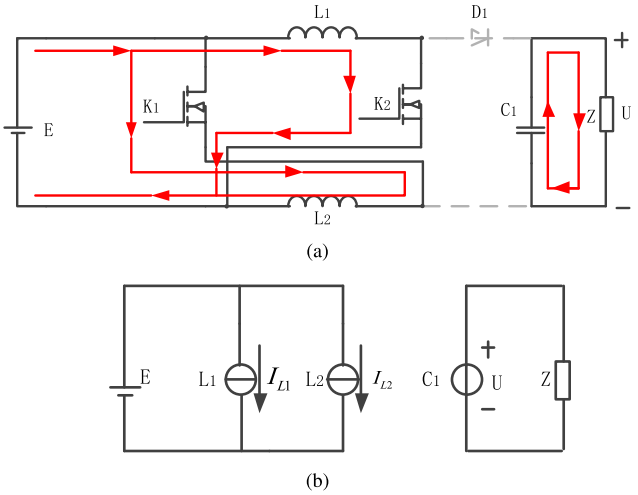

FIGURE 2. Operating mode and equivalent circuit of proposed dual-switch boost DC–DC converter when MOSFET are set in ON state. a) Working mode. b) Equivalent circuit.

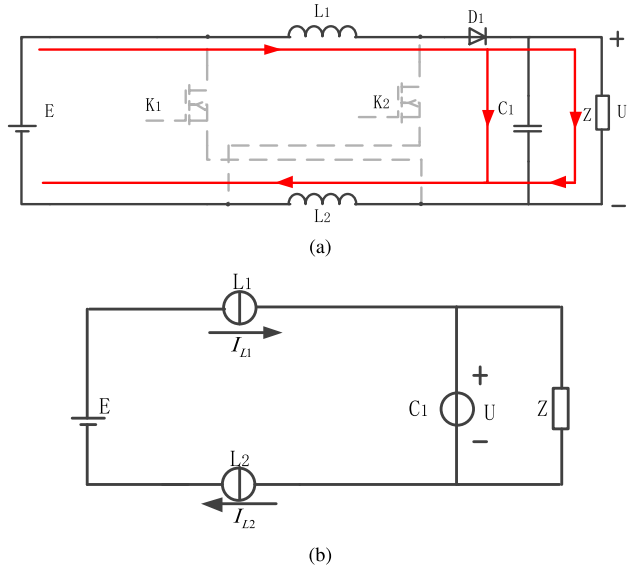

FIGURE 3. Operating mode and equivalent circuit of proposed dual-switch boost DC–DC converter with MOSFETs set in OFF state. a) Working mode. b) Equivalent circuit.

equal (i.e., $I_{L1} = I_{L2} = I_L$), the energy absorbed by inductors L_1 and L_2 can be expressed as

$$W_L = E \times I_L \times D \times TS \tag{1}$$

When the switch tube is set in the OFF state, the input voltage E exists in a series connection with inductors L_1 and L_2. In this state, energy is supplied to the filter capacitor C_1 and load Z through diode D_1, and the capacitor replenishes energy. The corresponding working mode of the proposed converter circuit is depicted in Figure 3(a). In this condition, the converter circuit exists as a single loop comprising inductors L_1 and L_2, input voltage E, diode D_1, filter capacitor C_1, and load Z. Ignoring the voltage drop across D_1, the equivalent circuit in this case corresponds to that depicted in Figure 3(b). As can be observed, in this condition, voltage directions across inductors L_1 and L_2 remain unrelated to corresponding current directions over the period during which energy is released. This released energy by each inductor can be expressed as

$$W'_L = \left(\frac{U-E}{2}\right) \times I_L \times (1-D) \times TS \tag{2}$$

In accordance with the principle of energy conservation, energies absorbed and released by the inductor during one PWM cycle must be equal.

$$W_L = W'_L \tag{3}$$

Solving equations (1), (2), and (3), voltage gain of the proposed dual-switch boost converter under ideal conditions can be expressed as

$$U = \frac{1+D}{1-D} \cdot E \tag{4}$$

Figure 4 depicts the relationship between the boost ratio and MOSFET duty cycle with regard to the proposed dual-switch boost DC–DC converter.

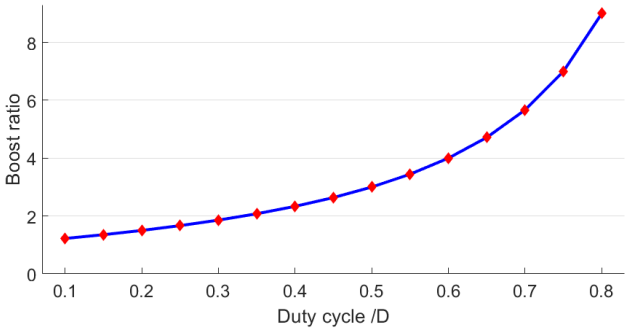

FIGURE 4. Relationship between boost ratio of dual-switch boost converter and duty cycle of MOSFET switch.

III. CONVERTER MODE OF OPERATION

To facilitate further analyze operating modes of the proposed converter topology, a state equation has been established in this study. The influence of inductor-current and capacitor-voltage fluctuations on converter operation must be considered when establishing the equation of state. Figure 5 depicts waveforms of different parameters concerning the proposed converter in operation.

As depicted in Figure 5, the interval t_1-t_0 corresponds to the ON state of the two MOSFETs—K_1 and K_2. During operation in this state, the diode D_1 remains in the OFF state, and the voltage-induced stress equals E + U. The voltage across inductors L_1 and L_2 corresponds to the input voltage E, and the inductor current increases linearly. Because the filter capacitor supplies energy to the load alone, the voltage across the capacitor must reduce. Considering inductor L_1 as an example, the change in current through it can be expressed as

$$L_1 \frac{dI_{L1}}{dt} = E \tag{5}$$

At t = D × TS, currents through L_1 and L_2 attain their respective maximum values, and the corresponding total

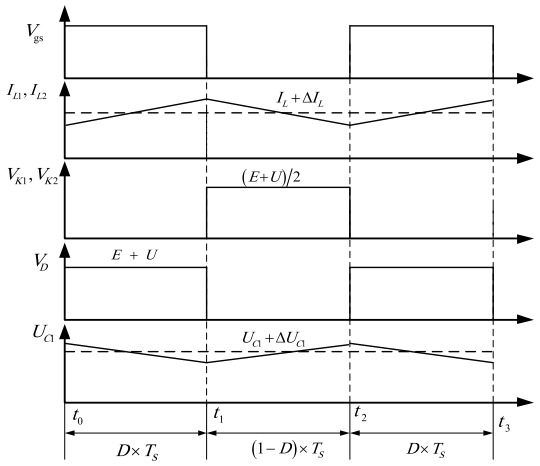

FIGURE 5. Parametric waveforms concerning proposed converter circuit in operation.

change in current can be expressed as

$$\Delta I_L^+ = \frac{E}{L} \times D \times TS \tag{6}$$

The change in voltage across capacitor C_1 is expressed as

$$C_1 \frac{dU_{C1}}{dt} = -\frac{U_{C1}}{Z} \tag{7}$$

Using the equation of state, the following equation can be deduced.

$$\begin{bmatrix} \frac{dI_{L1}}{dt} \\ \frac{dU_{C1}}{dt} \end{bmatrix} = \begin{bmatrix} 0 & 0 \\ 0 & -\frac{1}{C_1 \cdot Z} \end{bmatrix} \cdot \begin{bmatrix} I_{L1} \\ U_{C1} \end{bmatrix} + \begin{bmatrix} \frac{1}{L_1} \\ 0 \end{bmatrix} \cdot E \tag{8}$$

The interval $t_2 - t_1$ corresponds to the period during which both MOSFETs are set in the OFF state. When operating in this state, the diode D_1 is switched on, and the filter capacitor and load are energized simultaneously by both the input voltage and voltage across the inductor. Under this condition, the inductor current can be expressed as

$$-L_1 \frac{dI_{L1}}{dt} = \frac{U - E}{2} \tag{9}$$

The inductor current reduced to its lowest value at this stage, and the total change in inductor current can be expressed as

$$\Delta I_L^- = \frac{U - E}{2L} \times (1 - D) \times T_S \tag{10}$$

Correspondingly, the voltage across the capacitor increases owing to it being replenished with energy. The voltage equation for the capacitor C_1 can be expressed as

$$C_1 \frac{dU_{C1}}{dt} = I_{L1} - \frac{U_{C1}}{Z} \tag{11}$$

The state expression corresponding to this phase is

$$\begin{bmatrix} \frac{dI_{L1}}{dt} \\ \frac{dU_{C1}}{dt} \end{bmatrix} = \begin{bmatrix} 0 & -\frac{1}{2 \cdot L_1} \\ \frac{1}{C_1} & -\frac{1}{C_1 \cdot Z} \end{bmatrix} \cdot \begin{bmatrix} I_{L1} \\ U_{C1} \end{bmatrix} + \begin{bmatrix} \frac{1}{2 \cdot L_1} \\ 0 \end{bmatrix} \cdot E \tag{12}$$

To evaluate the performance of the proposed dual-switch boost DC–DC converter, operation of the proposed converter topology was compared against that of that of the boost, double-boost and quadratic-boost converters [18]–[20]. Assuming the power level, input voltage, and output current of the four topologies to be the same, the inductor-current ripple, output-voltage ripple, system frequency, and duty ratio were denoted by I_L, U, f, and D, respectively. Comparison indexes considered herein included the number of inductors, capacitors, switching tubes, diodes, maximum stress of switching tubes, maximum stress of diodes, maximum capacitance, maximum inductance, and theoretical boost ratio. Comparison results, so obtained, are described in Table 1.

Comparison and analysis of index values listed in Table 1 demonstrates that although the boost circuit comprises the least number of devices, its potential for realization of a high boost ratio is small. Theoretically, the quadratic-boost circuit provides the highest boost ratio; however, its implementation requires the most number of devices, and its structure is highly complicated. The double-boost and proposed dual-switch boost topologies provide nearly identical boost ratios and switching-tube stresses, and both offer their own advantages in terms of diode stress, capacitance and inductance parameters, and number of devices. The number of the two sides offers its own advantages; however, control of the two switches in the double-boost topology requires two PWMs with a phase difference of 180°, whereas the proposed dual-switch boost converter requires only a single PWM wave for switching control, and the difficulty associated with the said control is greatly reduced.

For boost circuits, the slopes of the inductance current rise (angle u) and fall (angle d) as follows:

$$\left(\frac{dI_L}{dt}\right)_u = \frac{U_{in}}{L} \tag{13}$$

$$\left(\frac{dI_L}{dt}\right)_d = \frac{U_{in} - U_C}{L} \tag{14}$$

Therefore, if f_{sw} is the switching frequency, the inductor current ripple of the boost circuit is:

$$\Delta I_L = \frac{D \cdot U_{in}}{L \cdot f_{sw}} \tag{15}$$

For the dual-switch boost converter, the total current ripple is:

$$\Delta I_2 = \begin{cases} \frac{1 - 2D}{1 - D} \Delta I_L, & 0 \le D \le 0.5; \\ \frac{2D - 1}{D} \Delta I_L, & 0.5 < D \le 1. \end{cases} \tag{16}$$

IV. EXPERIMENTAL VALIDATION

Major parameters concerning the performance of the proposed dual-switch boost converter are the input voltage (20 V), rated output voltage (100 V), rated output power (100 W), and switching frequency (20 kHz).

TABLE 1. Comparison of indicators in four topologies.

	Boost	Double-boost	Secondary-boost	Double tube-boost
Number of inductors	1	2	2	2
Number of capacitors	1	2	2	1
Number of switches	1	2	1	2
Number of diodes	1	2	3	1
Total number of devices	4	8	8	6
Switch tube stress	U_o	$(U_o+U_{in})/2$	U_o	$(U_o+U_{in})/2$
Diode stress	U_o	$(U_o+U_{in})/2$	U_o	(U_o+U_{in})
Capacitor	$I_{out}D/(\Delta U \times f)$	$I_{out}D/(2\Delta U \times f)$	$I_{out}D/(\Delta U \times f)$	$I_{out}D/(\Delta U \times f)$
Inductor	$U_{in}D/(\Delta I_L \times f)$	$U_{in}D/(2\Delta I_L \times f)$	$U_{in}D/(\Delta I_L \times f)$	$U_{in}D/(\Delta I_L \times f)$
Theoretical boost ratio	1/(1-D)	(1+D)/(1-D)	$1/(1-D)^2$	(1+D)/(1-D)

The calculation formulas of the inductors L1 and L2 are:

$$L_1 = L_2 = \frac{E \times D}{2 \times \Delta I_{IN} \times f} \tag{17}$$

ΔI_{IN} is the input current fluctuation and it takes the value of 20% of the average current.

The calculation formula of capacitors C is:

$$C = \frac{I_{out} \times D}{\Delta U \times f} = 35\mu F \tag{18}$$

Substituting the experimental prototype design indicator into equation (18), after calculation, the capacitor with a capacitance of 47 μF and a withstanding voltage of 400 V was selected.

After the previous analysis and calculation, the switch tube withstand voltage value is 60V.In this paper, the power MOSFET of the model IRF640N is selected as the switching tube. Its maximum on-current is 18A, and the maximum withstand voltage is 200V. The diode withstands a reverse voltage drop of U-E and an output current of 1A. Considering the margin of 2-3 times, The diode of the model DFE10I600PM is selected. Its maximum reverse voltage is 600V, conduction current is 10A, and maximum forward voltage drop is 1.5V.

The design prototype of the dual-switch boost converter topology, as depicted in Figure 6, comprises a main circuit, driving circuit, detecting circuit, an overcurrent-protection circuit, and an auxiliary power supply. During experiments performed in this study, the output load was simulated using a braking resistor and a sliding varistor box. A value of the boost ratio was determined in the open-loop state of the proposed device and subsequently compared against that observed during operation of the boost circuit. During tests, efficiency of the proposed device was observed to change in response to changes in operating conditions, such as load and output voltage. By comparing the ideal and actual boost ratios of the dual-switch boost converter against those of the

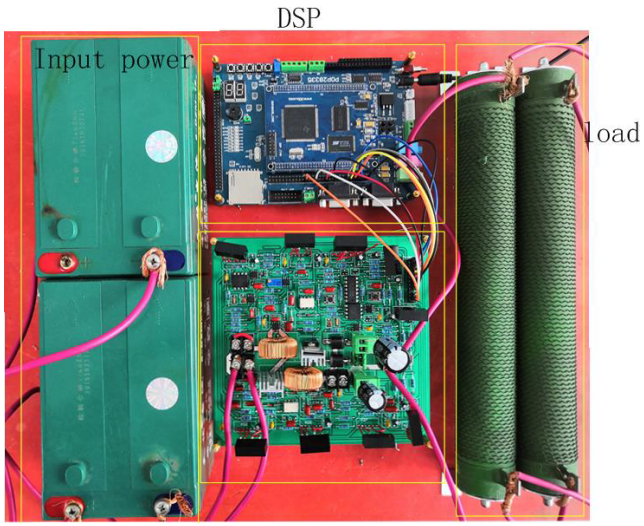

FIGURE 6. Designed power-module prototype of proposed dual-switch boost DC–DC converter.

boost circuit, advantages offered by the proposed converter topology can be summarized.

To further demonstrate the difference between actual and theoretical (ideal) boost ratios, boost-ratio versus duty-cycle curves corresponding to the ideal and actual operating states of the boost circuit and proposed dual-switch boost converter have been plotted in Fig. 7.

As can be observed in Fig. 7, ideal and actual boost ratios for both devices increase with increase in duty-cycle values from 0.2 to 0.8. At small duty-cycle values, actual boost-ratio curves for both devices nearly coincide with corresponding ideal curves, and the difference between the ideal and actual curves increases at high duty-ratio values. At a duty-cycle value of 0.8, differences between ideal and actual boost-ratio values concerning the boost circuit and proposed dual-switch

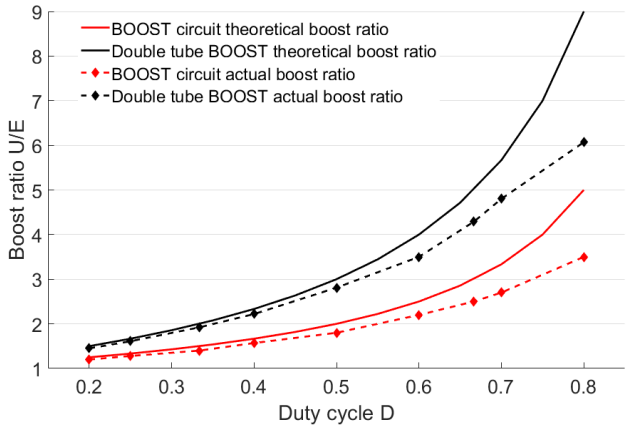

FIGURE 7. Comparison between ideal an actual boost ratios of the boost circuit and proposed dual-switch boost converter.

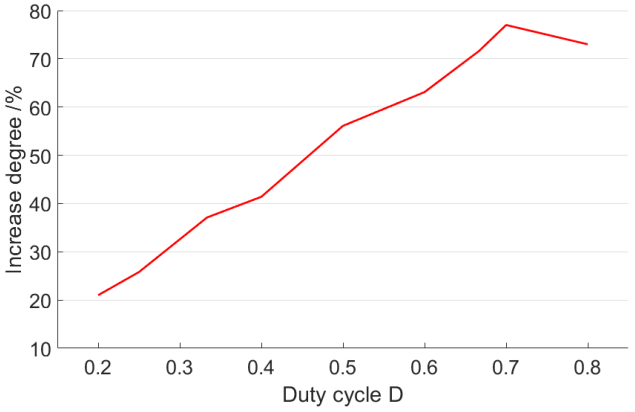

FIGURE 8. Improvement in boost ratio of dual-switch boost converter relative to boost circuit.

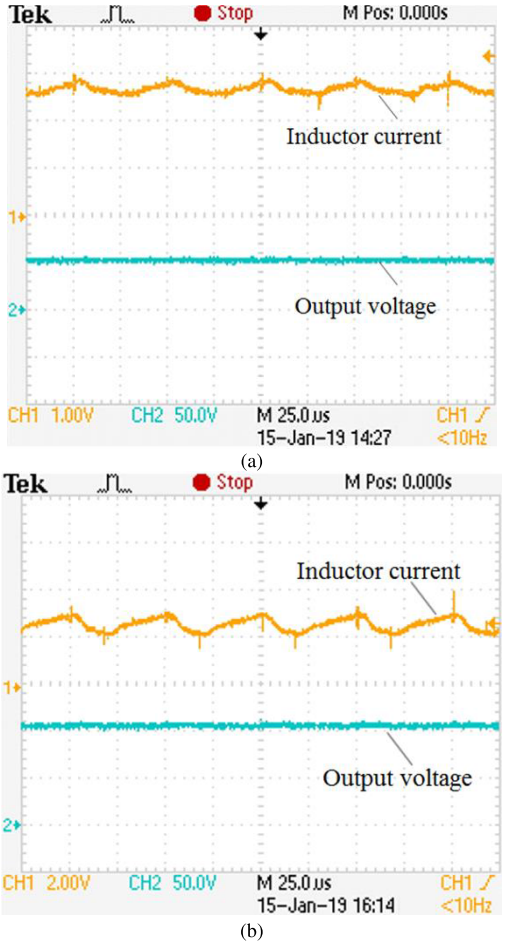

FIGURE 9. Output voltage and inductor current waveforms at different reference voltages. a) Uref = 50 V. b) Uref = 100 V.

boost converter are of the order of 30% and 33%, respectively. This indicates that simply increasing the duty cycle in boost converters does not correspond to realization of improved boost ratios. Novel converter topologies—capable of enhancing the boost ratio whilst reducing the duty cycle—therefore, need to be developed to facilitate their use in high-boost-ratio applications. The improvement in boost ratio of the proposed dual-switch boost converter relative to the boost circuit is depicted in Fig. 8.

As can be observed in Fig. 8, the degree of improvement in boost ratio of the proposed dual-switch boost converter relative to the boost circuit is not a monotonic function of the duty ratio D. At values of $D < 0.7$, the degree of improvement demonstrates a monotonic increase. At $D = 0.7$, the degree of improvement attains its maximum value of 77%, following which any further increase in D (i.e., $D > 0.7$) results in a decline in the observed degree of improvement.

When the input voltage is 24 V and the load is 100Ω, the output voltage waveform and inductance current waveform are shown in Fig. 5-6 when the output voltage is 50 V and 100 V respectively. The inductor current is converted into a voltage signal by the Hall sensor, and the measurement mode of the oscilloscope is an automatic measurement mode.

It can be seen from Fig. 9 that after the system reaches steady state, the output voltage remains unchanged, and the inductor current fluctuates up and down. And as the output voltage increases, the fluctuation amplitude of the inductor current increases. When the inductance current increases, it corresponds to the switch on stage, and when the current inductance decreases, it corresponds to the switch off state. The relationship between the output voltage U and the inductance current I_L in the switching off stage is $U = E + 2 \cdot L \cdot \frac{di_l}{dt}$. Therefore, if the output voltage is increased, the fluctuation of inductance current will increase accordingly.

Output-voltage waveforms corresponding to the proposed dual-switch boost converter and boost circuit under operating conditions defined by input and output voltages of 6 V and 20 V, respectively, are depicted in Fig. 10. As can be observed, output-voltage ripple coefficient concerning the proposed dual-switch boost converter equals 0.01, and its corresponding value for the boost circuit equals 0.015.

When the input voltage is 24V and the load is 100Ω, the output voltage of the dual-switch boost converter changes from 30V to 100V, the efficiency change and the boost converter are compared as shown in Figure. 11. Since the duty cycle range of the two types of boost converters is

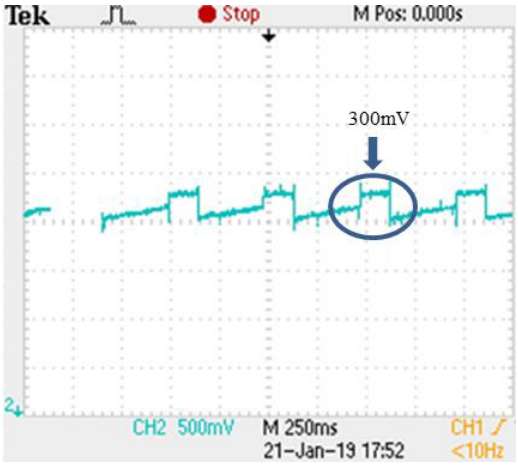

(a)

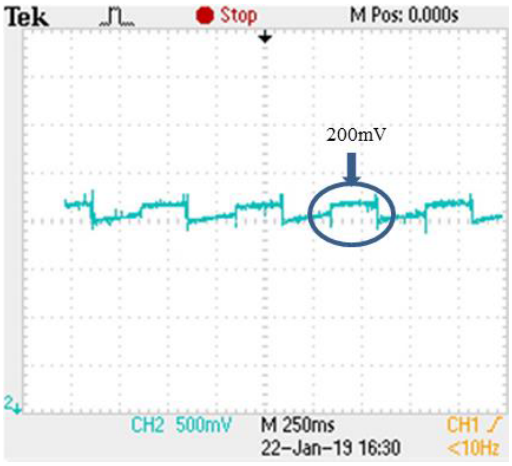

(b)

FIGURE 10. Output-voltage waveforms concerning the boost circuit and proposed converter topology. a) Boost converter. b) Dual-switch boost converter.

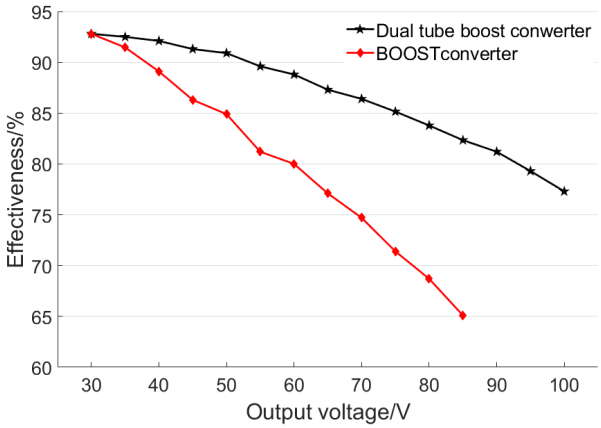

FIGURE 11. Comparison of efficiency between two types of boost converters.

set to 0.2 to 0.8, the boost range of the boost converter is 30V to 85V.

As can be seen in Fig. 11, at a constant output load, efficiencies of the proposed dual-switch boost converter and boost circuit demonstrate reduction with increase in output voltage with continuous increase in the rate of reduction. The proposed dual-switch boost converter demonstrates an efficiency of 92.8% at an output voltage of 30 V, and that of efficiency of approximately 77.3% when the output voltage equals 100 V. The boost circuit, on the other hand, demonstrates an efficiency of 92.5% at an output voltage of 30 V, and at an output voltage of 85 V, its corresponding minimum efficiency equals 65.1%. Thus, at all output voltages, efficiency of the proposed dual-switch boost converter exceeds that of the conventional boost circuit, and the larger the output voltage, the greater is the difference between efficiencies of the two devices. This may be attributed to the fact that power consumption of the boost circuit is related to the inductor current and duty cycle. With increase in output voltage, the duty cycle D and inductor current continue to increase, thereby resulting in an increase in inductance loss, losses within the switching tube, and reduced system efficiency [21].

When the output voltage is set to 50 V and load resistance is varied over the range of 50–100 Ω, efficiencies of the proposed dual-switch boost converter and boost circuit compare as depicted in Fig. 12.

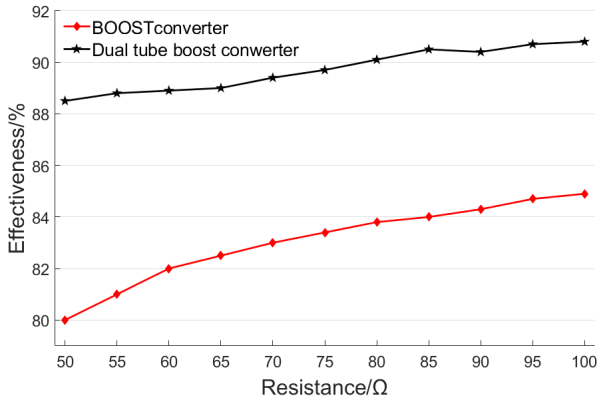

FIGURE 12. Efficiency trends concerning proposed converter and boost circuit under varying load resistances and 50-V output voltage.

When the output voltage equals 50 V, the efficiency of the conventional boost circuit increases with increase in load resistance. As depicted in the figure, boost-circuit efficiencies corresponding to load-resistance values of 50 Ω and 100 Ω approximately equal 80% and 84.9%, respectively. On the other hand, efficiency of the proposed dual-switch boost converter continuously increases with increase in load resistance from 50 Ω to 85 Ω, at which point the efficiency increase becomes nearly insignificant, and the device efficiency becomes nearly constant at 90.5%. The overall circuit loss depends on the ON-state current flowing through the device and corresponding ON time of the device. The larger the duty cycle and ON-state current, the greater is the conduction loss incurred [22]. With increase in load resistance, the output current decreases, and the conduction and inductance losses associated with the switching tube are reduced. Consequently, efficiencies of both types of boost converters can be observed to be improved.

V. CONCLUSIONS

This paper describes the development and demonstrates the utility of a DC–DC converter topology based on a double-tube-boost structure to satisfy the requirements of high gain and wide range of operation of DC–DC converters employed in fuel-cell-based vehicle-power-system applications. By comparing the proposed converter topology against different step-up DC–DC converters, the following conclusions have been drawn from this study.

(1) With regard to the number of circuit components, boost ratio, and switching-tube stress, the proposed dual-switch boost converter offers numerous advantages over the conventional, double, and cascaded boost circuits. The operating principle of the proposed converter is simple, and control over its operation can be easily realized via one-way PWM.

(2) At any given output voltage, the proposed converter achieves an efficiency higher compared to that of the traditional boost circuit. As observed during comparisons, the larger and smaller the output voltage and current, respectively, the more does the proposed-converter efficiency exceed that of the booster circuit.

REFERENCES

[1] E. M. Barhoumi, I. B. Belgacem, A. Khiareddine, M. Zghaibeh, and I. Tlili, "A neural network-based four phases interleaved boost converter for fuel cell system applications," *Energies*, vol. 11, no. 12, p. 3423, 2018.

[2] T. H. Eom, J.-W. Kang, J. Kim, M.-H. Shin, J.-H. Lee, and C.-Y. Won, "Improved voltage drop compensation method for hybrid fuel cell battery system," *Electronics*, vol. 7, no. 11, p. 331, 2018.

[3] K. J. Reddy and S. Natarajan, "Energy sources and multi-input DC–DC converters use in hybrid electric vehicle applications—A review," *Int. J. Hydrogen Energy*, vol. 43, no. 36, pp. 17387–17408, 2018.

[4] L. Xu, P. Hong, C. Fang, J. Li, M. Ouyang, and W. Lehnert, "Interactions between a polymer electrolyte membrane fuel cell and boost converter utilizing a multiscale model," *J. Power Sources*, vol. 395, pp. 237–250, Aug. 2018.

[5] M. Forouzesh, Y. P. Siwakoti, S. A. Gorji, F. Blaabjerg, and B. Lehman, "Step-up DC–DC converters: A comprehensive review of voltage-boosting techniques, topologies, and applications," *IEEE Trans. Power Electron.*, vol. 32, no. 12, pp. 9143–9178, Dec. 2017.

[6] M. R. Banaei and S. G. Sani, "Analysis and implementation of a new SEPIC-based single-switch buck–boost DC–DC converter with continuous input current," *IEEE Trans. Power Electron.*, vol. 33, no. 12, pp. 10317–10325, Dec. 2018.

[7] Q. Wu, Q. Wang, Q. Li, and Z. Wang, "ZVS three-phase current-fed push–pull converter employing a simple active-clamp circuit for voltage step-up applications," *IET Power Electron.*, vol. 11, no. 14, pp. 2286–2294, 2018.

[8] S. Talebi, E. Adib, and M. Delshad, "A high gain soft switching interleaved DC–DC converter," *IEICE Trans. Electron.*, vol. E101C, no. 11, pp. 906–915, 2018.

[9] M. Yaqoob, K. Loo, and Y. M. Lai, "Fully soft-switched dual-active-bridge series-resonant converter with switched-impedance-based power control," *IEEE Trans. Power Electron.*, vol. 33, no. 11, pp. 9267–9281, Nov. 2018.

[10] A. Rajaei, R. Khazan, M. Mahmoudian, M. Mardaneh, and M. Gitizadeh, "A dual inductor high step-up DC/DC converter based on the Cockcroft–Walton multiplier," *IEEE Trans. Power Electron.*, vol. 33, no. 11, pp. 9699–9709, Nov. 2018.

[11] H. Bi, P. Wang, and Y. Che, "H-type structural boost three-level DC-DC converter with wide voltage-gain range for fuel cell applications," *J. Power Electron.*, vol. 18, no. 5, pp. 1303–1314, 2018.

[12] W. Sun, Y. Xing, H. Wu, and J. Ding, "Modified high-efficiency LLC converters with two split resonant branches for wide input-voltage range applications," *IEEE Trans. Power Electron.*, vol. 33, no. 9, pp. 7867–7879, Sep. 2018.

[13] Y. Zhang, L. Zhou, M. Sumner, and P. Wang, "Single-switch, wide voltage-gain range, boost DC–DC converter for fuel cell vehicles," *IEEE Trans. Veh. Technol.*, vol. 67, no. 1, pp. 134–145, Jan. 2018.

[14] Q. Wu, Q. Wang, J. Xu, and L. Xiao, "Implementation of an active-clamped current-fed push–pull converter employing parallel-inductor to extend ZVS range for fuel cell application," *IEEE Trans. Ind. Electron.*, vol. 64, no. 10, pp. 7919–7929, Oct. 2017.

[15] P. Wang, L. Zhou, Y. Zhang, J. Li, and M. Sumner, "Input-parallel output-series DC–DC boost converter with a wide input voltage range, for fuel cell vehicles," *IEEE Trans. Veh. Technol.*, vol. 66, no. 9, pp. 7771–7781, Sep. 2017.

[16] S. Hiranuma, T. Takayanagi, N. Hoshi, J. Haruna, and M. Cao, "Experimental consideration on DC–DC converter circuits for fuel cell hybrid electric vehicle," in *Proc. Elect. Vehicle Conf.*, 2012, pp. 1–8.

[17] L.-S. Yang, T.-J. Liang, and J.-F. Chen, "Transformerless DC–DC converters with high step-up voltage gain," *IEEE Trans. Ind. Electron.*, vol. 56, no. 8, pp. 3144–3152, Aug. 2009.

[18] H. Wu, T. Mu, H. Ge, and Y. Xing, "Full-range soft-switching-isolated buck-boost converters with integrated interleaved boost converter and phase-shifted control," *IEEE Trans. Power Electron.*, vol. 31, no. 2, pp. 987–999, Feb. 2016.

[19] J. Liu, D. Gao, and Y. Wang, "High power high voltage gain interleaved DC–DC boost converter application," in *Proc. 6th Int. Conf. Power Electron. Syst. Appl. (PESA)*, Dec. 2015, pp. 1–6.

[20] X. Liu, X. Li, Q. Zhou, and J. Xu, "Flicker-free single-switch quadratic boost LED driver compatible with electronic transformers," *IEEE Trans. Ind. Electron.*, vol. 66, no. 5, pp. 3458–3467, May 2019.

[21] A. Ayachit and M. K. Kazimierczuk, "Averaged small-signal model of PWM DC-DC converters in CCM including switching power loss," *IEEE Trans. Circuits Syst. II, Exp. Briefs*, vol. 66, no. 2, pp. 262–266, Feb. 2019.

[22] A. Mallik and A. Khaligh, "Maximum efficiency tracking of an integrated two-staged AC–DC converter using variable DC-link voltage," *IEEE Trans. Ind. Electron.*, vol. 65, no. 11, pp. 8408–8421, Nov. 2018.

XIAOGANG WU was born in Heilongjiang, China. He received the M.E. and Ph.D. degrees in power electronics and power drive from the Harbin University of Science and Technology, Harbin, China, in 2006 and 2009, respectively.

From 2010 to 2012, he held a postdoctoral position with at Tsinghua University, Beijing, China. He is currently a Professor with the Harbin University of Science and Technology. His research interests include optimization matching and energy management of hybrid power systems, power battery charge management, and electric vehicle access technology.

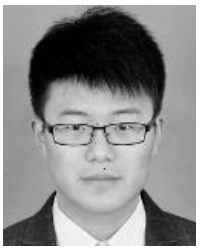

WENWEN SHI was born in Shandong, China. He received the B.E. degree in electrical engineering and automation from the Qingdao University of Technology, Qingdao, China, in 2014. He is currently pursuing the M.E. degree in electrical engineering with the Harbin University of Science and Technology, Harbin, China.

His research interest includes the battery management systems in electric vehicles.

JIUYU DU received the Ph.D. degree with the School of Mechanical Engineering, Beijing Institute of Technology, Beijing, China, in 2009.

From 2009 to 2012, she held a Postdoctoral at Tsinghua University, Beijing, China, where she is currently an Associate Professor with the Department of Automotive Engineering. Her research interests include power battery management and electric vehicle technology.